Deuterium Abundance Toward WD 2211−495: Results from the Far Ultraviolet Spectroscopic Explorer (*FUSE*) Mission [1]

G. Hébrard[2]; M. Lemoine, A. Vidal-Madjar, J.-M. Désert,

A. Lecavelier des Étangs, R. Ferlet

Institut d'Astrophysique de Paris, 98^{bis} boulevard Arago, F-75014 Paris, France

B. E. Wood, J. L. Linsky

JILA, University of Colorado and NIST, Campus Box 440, Boulder, CO 80309-0440, USA

J. W. Kruk, P. Chayer[3], S. Lacour, W. P. Blair,

S. D. Friedman, H. W. Moos, K. R. Sembach

Department of Physics and Astronomy, Johns Hopkins University, Baltimore, MD 21218, USA

G. Sonneborn, W. R. Oegerle

Laboratory for Astronomy and Solar Physics, NASA/GSFC, Code 681, Greenbelt, MD 20771, USA

and

E. B. Jenkins

Princeton University Observatory, Princeton, NJ 08544, USA

Received _____; accepted _____

---

[2]email: hebrard@iap.fr

[3]Primary affiliation: Department of Physics and Astronomy, University of Victoria, P.O. Box 3055, Victoria, BC V8W 3P6, Canada.

ABSTRACT

We present a deuterium abundance analysis of the line of sight toward the white dwarf WD 2211−495 observed with the Far Ultraviolet Spectroscopic Explorer (*FUSE*). Numerous interstellar lines are detected on the continuum of the stellar spectrum. A thorough analysis was performed through the simultaneous fit of interstellar absorption lines detected in the four *FUSE* channels of multiple observations with different slits. We excluded all saturated lines in order to reduce possible systematic errors on the column density measurements. We report the determination of the average interstellar D/O and D/N ratios along this line of sight at the 95% confidence level: $D/O = 4.0\,(\pm 1.2) \times 10^{-2}$; $D/N = 4.4\,(\pm 1.3) \times 10^{-1}$. In conjunction with *FUSE* observations of other nearby sight lines, the results of this study will allow a deeper understanding of the present-day abundance of deuterium in the local interstellar medium and its evolution with time.

Subject headings: ISM: abundances – ISM: clouds – cosmology: observations – ultraviolet: ISM – stars: individual (WD2211-495) – (stars:) white dwarfs

1. Introduction

Deuterium is believed to be produced in appreciable quantities only in primordial Big Bang nucleosynthesis (BBN) and destroyed in stellar interiors (*e.g.*, Epstein et al. 1976); it is

[1]Based on observations made with the NASA-CNES-CSA Far Ultraviolet Spectroscopic Explorer. *FUSE* is operated for NASA by the Johns Hopkins University under NASA contract NAS5-32985.

thus a key element in cosmology and in galactic chemical evolution (see *e.g.* Vangioni-Flam & Cassé 1995; Prantzos 1996; Scully et al. 1997). The primordial abundance of deuterium is one of the best probes of $\Omega_B h^2$, the baryonic density of the Universe divided by the critical density. The abundance of deuterium relative to hydrogen (D/H) is expected to decline during Galactic evolution at a rate that is a function of the star formation rate; standard models predict a factor of 2 to 3 decrease in the deuterium abundance in 15 Gyrs (see *e.g.*, Galli et al. 1995; Tosi et al. 1998). Hence, any abundance of deuterium measured at any metallicity should provide a lower limit to the primordial deuterium abundance. This picture is essentially constrained by deuterium abundance measurements at look-back times of $\sim$ 14 Gyrs (primordial intergalactic clouds), 4.5 Gyrs (protosolar), and 0.0 Gyrs (interstellar medium). Although the evolution of the deuterium abundance seems to be qualitatively understood, measurements of D/H at similar redshifts show some dispersion and indicate that additional processes may be important in controlling the abundance of deuterium. That fact has led to the development of non-standard models, which propose, for example, larger astration factors (*e.g.*, Vangioni-Flam et al. 1994) or non-primordial deuterium production (see *e.g.*, Lemoine et al. (1999) for a review).

Up to now, the interstellar medium is the astrophysical site that has allowed the most comprehensive investigations of deuterium abundances. Deuterium has been observed in the interstellar medium using different methods: radio measurements of its 92 cm hyperfine transition (*e.g.*, Blitz & Heiles 1987; Chengalur et al. 1997), observations of deuterated molecules (*e.g.*, Lubowich et al. 2000; Ferlet et al. 2000), Balmer series analyses (Hébrard et al. 2000), and Lyman series absorption (see Moos et al. 2001). Of these, the most accurate measurements have been obtained through Lyman absorption-line observations in the far-ultraviolet (far-UV) spectral range. By observing hydrogen and deuterium directly in their atomic form, far-UV Lyman series absorption-line measurements provide accurate column density determinations that are not dependent on ionization or

chemical fractionation effects. The first measurement of the abundance ratio $(D/H)_{ISM}$ was reported by Rogerson & York (1973) for the line of sight to β Cen, using *Copernicus*: $(D/H)_{ISM} = 1.4 \pm 0.2 \times 10^{-5}$. Since then, many other $(D/H)_{ISM}$ measurements have been performed using different instruments (*Copernicus*, *IUE*, *IMAPS*, *HST*) for other sight lines, and the values obtained show significant dispersion around the above value.

For example, an average value $(D/H)_{ISM} = 1.50(\pm 0.10) \times 10^{-5}$ $(1\,\sigma)$ has been derived for the Local Interstellar Cloud (Lallement & Bertin 1992) by Linsky (1998) from the comparison of 12 nearby sight lines, but studies of several lines of sight revealed values outside this range (*e.g.*, Laurent et al. 1979; York 1983; Allen et al. 1992; Vidal-Madjar et al. 1998; Hébrard et al. 1999; Jenkins et al. 1999; Sonneborn et al. 2000). This dispersion may result from spatial variations due to some unknown physical processes or underestimation of systematic errors. There is still considerable debate over these two interpretations, and the final resolution of the issue may have implications for understanding the physics of the interstellar medium, as well as the baryonic density inferred from D/H measurements. Measurements of D/H in the intergalactic medium are also sparse and do not agree with each other (*e.g.*, Webb et al. 1997; Burles & Tytler 1998a; 1998b), so an accurate determination of the primordial deuterium abundance has also proven to be a difficult quantity to measure. Moreover, recent studies of the anisotropy of the cosmic microwave background (CMB), which permits evaluations of the baryonic density independent of those obtained through deuterium measurements (see, *e.g.*, de Bernardis et al. 2000; Jaffe et al. 2001), imply higher values of $\Omega_B h^2$ than those implied by the abundance studies, corresponding to a primordial D/H value of the order of the $(D/H)_{ISM}$ values (see however de Bernardis et al. 2001; Stompor et al. 2001; Pryke et al. 2001).

An accurate determination of the interstellar deuterium abundance is one of the main objectives of the Far Ultraviolet Spectroscopic Explorer (*FUSE*), which was successfully

launched on 1999 June 24 (Moos et al. 2000). In this paper, we present new measurements of deuterium abundances obtained with *FUSE* toward the white dwarf WD 2211−495. This paper is part of a series dedicated to *FUSE* measurements of deuterium interstellar abundances toward BD +28° 4211 (Sonneborn et al. 2001), WD 1634−573 (Wood et al. 2001), WD 0621−376 (Lehner et al. 2001), G191−B2B (Lemoine et al. 2001), HZ 43A (Kruk et al. 2001), and Feige 110 (Friedman et al. 2001). A major goal of this program is to determine to what extent and on what scales variations in the D/H ratio occur. Moos et al. (2001) present an overview of these first results.

White dwarfs are ideal targets for the measurement of the interstellar deuterium abundance (Lemoine et al. 1996); they may be chosen close to the Sun (so that the column densities are not too high and the velocity structure of the line of sight is not too complex), and they exhibit relatively smooth UV continua (which allow detections of lines from many species). Prior to this series of papers, measurements have been published for $(D/H)_{ISM}$ toward three white dwarfs: G191−B2B (Lemoine et al. 1996; Vidal-Madjar et al. 1998; Sahu et al. 1999), Sirius-B (Hébrard et al. 1999), and Feige 24 (Vennes et al. 2000).

The *FUSE* observations of WD 2211−495 and the data processing are presented in Sect. 2, and the details of the analysis in Sect. 3. The results are reported in Sect. 4 and discussed in Sect. 5.

2. Observations and data processing

WD 2211−495 (RE J2214−491) was identified by the *ROSAT* wide field camera all-sky survey as an extreme ultraviolet source and was classified as a new white dwarf star (Pounds et al. 1993). Holberg et al. (1993) analyzed the optical and high-resolution International Ultraviolet Explorer (*IUE*) spectra of WD 2211−495 and concluded it was a hot DA white

dwarf showing traces of heavy elements such as C, N, O, Si, and Fe. Later, Holberg et al. (1994) and Werner & Dreizler (1994) discovered the presence of Ni in the co-added *IUE* spectrum, confirming that WD 2211−495 was one of the most metal-rich white dwarfs known. Barstow et al. (1998) determined the atmospheric parameters of the star by considering non-LTE metal-line-blanketed model atmospheres and found $T_{\rm eff}$ = 62,000 K and $\log g = 7.2$. WD 2211−495 has a mass $M \simeq 0.53$ $M_{\odot}$ according to optical spectroscopic analyses performed by Marsh et al. (1997a), Vennes et al. (1997), and Finley et al. (1997). Its photometric distance is $d \simeq 53$pc (Holberg et al. 1998). Table 1 summarizes relevant sight line and atmospheric parameters for WD 2211−495.

2.1. Observations

WD 2211−495 was observed in 1999 and 2000 as part of the *FUSE* photometric calibration program and the *FUSE* Science Team D/H program. Seventeen observations consisting of 188 individual exposures for a total exposure time of 93 800 sec ($\sim$ 26 hours) were used in the present study. All the observations were obtained in histogram mode, through one of the three slits available (Moos et al. 2000): the large (LWRS), medium (MDRS), or high resolution aperture (HIRS). Table 2 shows the log of the observations used in this analysis.

2.2. Data processing

The one-dimensional spectra were extracted from the two-dimensional detector images and calibrated using slightly different versions of the `CALFUSE` pipeline (see Table 2), depending of the version available in the archives for a given observation. For a given slit (LWRS, MDRS, or HIRS), data from each channel and segment (SiC1A, SiC2B, LiF1A,

LiF2B, etc.) were co-added separately, after wavelength shift corrections of the individual calibrated exposures. Wavelength shifts between individual spectra were typically a few pixels for exposures of a given observation and a few tens of pixels between exposures of different observations. Because a given wavelength falls on different pixels in different exposures, co-addition of the numerous exposures results in a considerable reduction in fixed-pattern noise (Sahnow et al. 2000) by acting like a random FP-Split procedure (Kruk et al. 2001).

Exposures with strong airglow emission, large spectral resolution variations, or large wavelength stretching[4] were not included in the sums. The last two criteria were applied in particular to the two observations performed in 1999, early in the mission. In order to properly co-add different exposures for a given segment, the same wavelength calibration file (`wave*009`) was used in `CALFUSE` for all of the observations. That led us to re-run `CALFUSE` in the version 1.8.7 (which includes `wave*009`) for the observations which were archived in an older version which did not include this calibration file (see Table 2). The spectral resolution in the final spectra ranges between $\sim$ 13000 and $\sim$ 18500, depending on detector segment and wavelength (see Section 4.1).

All of the spectra were binned to three pixel samples (the line spread function (LSF) is about 10 pixels wide). The final LWRS spectra are plotted in Figure 1; similar datasets were obtained for the MDRS and HIRS slits. A sample of a spectrum (SiC1B with LWRS) is shown in Figure 2 with the D I, O I, and N I lines identified.

---

[4]Wavelength stretchings are inconsistencies in the wavelength scale (Sahnow et al. 2000).

3. Data Analysis

3.1. Method overview

For a given transition of a given element, each interstellar cloud along the sight line produces an absorption line that can be modeled with a Voigt profile. In addition to atomic parameters [taken from Morton (1991; 1999)] a Voigt profile is defined by four cloud parameters: the radial velocity v of the cloud (in $\mathrm{km\,s^{-1}}$), the column density N_i of the element i (in $\mathrm{cm^{-2}}$), the temperature T of the gas (in K), and its micro-turbulent velocity ξ (in $\mathrm{km\,s^{-1}}$). *FUSE* does not have sufficient spectral resolution to resolve the individual velocity components along the WD 2211−495 sight line. This implies that *FUSE* cannot resolve the fine shape of individual velocity components and that it cannot reveal the presence of closely spaced multiple components. We do not have high-resolution ground-based interstellar data at our disposal for this star.

The analysis has been done using the profile fitting procedure `Owens.f`, developed by one of us (M.L.) and the *FUSE* French Team. A subset of the data has been independently fitted using a second procedure (see Sect. 4.2.2), developed by another of us (B.E.W.). The reader should refer to Wood et al. (2001) for a full description of this fitting procedure, and we will concentrate on describing in detail the results obtained with `Owens.f`.

`Owens.f` models Voigt profiles using χ^2 minimization. One of the characteristics of this procedure is that it is able to fit simultaneously several lines in different spectral windows, a spectral window being a part of a full spectrum (see Figures 3-6). Thus, this procedure finds the best solution compatible with numerous spectral lines based on the assumption that all lines considered yield the same values for v, T, and ξ for a given component, and that all lines for a specific component of element i give the same value for N_i. The width of the lines combines both parameters T and ξ, which can only be separately determined if

several elements with different masses are simultaneously fit[5].

Data at the edge of each detector segment are inaccurate (see Figure 1) and were not used in the fit. In the end, 32 different absorption lines (D I, O I, N I, Fe II, Si II, and P II) were modeled, which were observed in different segments and spectra, resulting in a total of 115 simultaneously fitted lines. Remaining ions like Ar I and N II were modeled separately in extra fits. No H_2 lines were detected. The 115 fitted lines are located in 65 different spectral windows, extracted from the different spectra, obtained through the HIRS, MDRS, and LWRS slits, on channels SiC1, SiC2, LiF1, and LiF2. Plots of the 65 spectral windows are shown in Figures 3-6. Atomic parameters of the D I, O I, and N I lines used are reported in Table 3.

3.2. Free parameters

All the cloud parameters (v, T, ξ and all the N_i's) were free to vary in the fit. We also allowed the continua shape, the spectral shift and the LSF width to vary from one spectral window to the next. These parameters are a priori unknown or poorly known, and this uncertainty is likely to introduce systematic effects in the final result. We take into account this uncertainty by treating these unknowns as free parameters in the fit, so that their uncertainty is included in the χ^2 variations (see Sect. 3.6).

The continua were fit by 3^{rd} to 7^{th} order polynomials (see Figures 3-6), depending on the spectral region. All the parameters of the polynomials were free. The spectral shift of each window[6] (*i.e.*, its wavelength zero point) was free to allow for possible inaccuracy of

---

[5]The b-value, which is the width of a line, is given by $b^2 = \frac{2kT}{m} + \xi^2$, where k is the Boltzmann constant and m the mass of the element.

[6]Actually, the spectral shift was free for all windows but one in order to avoid degeneracy

the *FUSE* wavelength calibration.

All Voigt profiles were convolved with a simple Gaussian LSF. The spectral resolution of *FUSE* is not accurately determined, but it is known to depend on the segment and wavelength. We let the width of the LSF vary freely for each spectral window. Note that fits with a double Gaussian LSF were also performed (see Sect. 4.2.2).

3.3. Unsaturated lines

Since we are primarily interested in abundances, we focused on the determination of column densities. We chose to use only unsaturated lines in the fits to reduce uncertainties resulting from saturation effects and other systematic errors. Saturated lines are not very sensitive to the column density. Since the lines which we use are on the linear part of the curve of growth, we can measure the total column densities for the line of sight even though the individual clouds are not resolved. All the H I interstellar lines detectable in the *FUSE* spectral range are located on the flat part of the curve of growth for this sight line; hence, no accurate H I column density could be determined. We thus determined D/O and D/N ratios instead of D/H. In order to fit the Lyman D I lines without fitting H I lines with Voigt profiles, the blue wings of the H I lines were fit with polynomials (see *e.g.*, Figure 5, left panel) to provide the continuum for D I absorption (see, however, Sect. 4.2.2).

3.4. Stellar model

We compared the *FUSE* spectrum of WD 2211−495 to a stellar model in order to verify that the interstellar lines were not blended with stellar lines. To this end, we computed

---

in a parameter space with the radial velocity of the absorber.

a non-LTE metal line-blanketed model atmosphere using the programs TLUSTY/SYNSPEC (Hubeny & Lanz 1995). We used the atmospheric parameters determined by Barstow et al. (1998) (see Table 1). We performed an abundance analysis using the *FUSE* and *IUE* data and then computed a synthetic spectrum incorporating these abundances (Chayer et al. 2001). The comparison between the stellar model and the *FUSE* spectrum allowed us to exclude the O I λ950.88Å and Si II λ989.87Å interstellar lines that are blended with the P IV λ950.66Å and N III λ989.80Å stellar lines. In agreement with the DA-type classification of the WD 2211−495, no He II absorption is seen in the *FUSE* spectrum (*e.g.*, λ1084.9Å or λ992.3Å), and hence such absorption should be absent at the intervening H I Lyman lines.

3.5. Zero flux level

To properly deduce abundances from interstellar absorption lines, it is extremely important to precisely evaluate the zero flux level. Although scattered light in *FUSE* is low (Moos et al. 2000; Sahnow et al. 2000), some residual flux is visible on the bottom of the H I Lyman lines, as one can see in Figures 1 and 2. This residual flux (at a level of few percent of the continuum) is probably due to the scatter of adjacent flux from the continuum due to the wings of the LSF. This interpretation agrees with the fact that this small amount of flux is not detected at wavelengths lower than the Lyman break, where there is no flux for scatter. Since the residual flux is so low, for each spectral window we tuned the zero flux level to the signal at the core of the nearest Lyman line, where it is readily measurable because these lines are totally saturated. The diffuse light is a few percent of the continuum, and its variations as a function of wavelength seem to be of the same order of magnitude, or even lower. Fits with a double Gaussian LSF were also performed (see Sect. 4.2.2).

3.6. χ^2 scaling and $\Delta\chi^2$ method

The χ^2 of the final fit was 2424.2. The difference between the number of independent spectral bins used in the fit and the number of free parameters (cloud, polynomials, shifts, and LSF parameters) was 1764. For this number of degrees of freedom, the reduced χ^2 is 1.37. This value is larger than 1.00, probably because of a small underestimation of the tabulated errors for each spectral bin. These errors are computed by the extraction pipeline which does not take into account all possible instrumental artifacts.

For each estimated parameter, *e.g.* N(D I), error bars were computed from an analysis of the χ^2 variation. We pegged that parameter at various trial values, and for each trial value we ran an extra fit, allowing all the other parameters to vary freely. We used these minima to define the confidence interval. Scanning the parameter in that way for different values (up to at least $\Delta\chi^2 = 50$), we obtained the value of χ^2 as a function of this parameter, and we derived the 1, 2, 3, 4, 5, 6, and 7 σ error bars using the standard $\Delta\chi^2$ method. The error bars at these different confidence levels have been taken into account to produce the final 2 σ uncertainties reported here. The $\Delta\chi^2$ curves as a function of column density are plotted in Figure 7.

However, since our best fit χ^2 value lies far above what would be expected for the corresponding number of degrees of freedom, and since that change is due to inaccurate estimates of the noise array, we rescaled our χ^2 and the corresponding $\Delta\chi^2$ values in the following way. At the 95% confidence level, the smallest value that one can draw from a χ^2 distribution with 1764 degrees of freedom is 1667.5, and consequently we increase the noise variance on each pixel by a factor $2424.2/1667.5 \simeq 1.45$ (2424.2 corresponds to our best fit value), or equivalently we divide our χ^2 and $\Delta\chi^2$ by a factor 1.45. Note that this is the most conservative choice at the 95% confidence level for the rescaling parameter. For example, for the 5 σ contour in χ^2 one should now look for differences $\Delta\chi^2 = 25 \times 1.45$

using our original error array, which corresponds to the standard $\Delta\chi^2 = 25$ for the correctly rescaled error array. This rescaling, similar to that presented by Lemoine et al. (2001), has increased in a conservative way the error bars derived below.

4. Results

4.1. Parameters values

Our column densities measurements are reported in Table 4. We derived the following abundance ratios:

$$\mathrm{D/O} = 4.0\ (\pm 1.2) \times 10^{-2}$$

$$\mathrm{D/N} = 4.4\ (\pm 1.3) \times 10^{-1}$$

with $2\,\sigma$ error bars. These error bars were computed from the individual errors on the column densities listed in Table 4, assuming that they are uncorrelated. Although the noise may not follow a Gaussian distribution, we checked on smooth parts of the spectrum that the tabulated error bars scaled as described above (Sect. 3.6) effectively include more than 95% of the individual points of the spectrum. Therefore, the quoted "$2\,\sigma$" error bars can be considered as a 95% confidence level, statistic and systematic effects being taking into account (see Sect. 4.2).

A formal temperature and turbulent velocity measured through the fit are $T = 3400 \pm 2500\mathrm{K}$ and $\xi = 3.0 \pm 1.0\mathrm{km\,s^{-1}}$. These values should be taken with caution because several velocity components may be present and the spectral lines are not resolved. It is also a combination between turbulent velocity and velocity dispersion of the possible

different clouds. In addition, these values were obtained from fits of unsaturated lines, which are not very sensitive to temperature and turbulent velocity.

For a given channel, the relative shifts between different spectral windows were found to be relatively constant, with a dispersion below 10 $\mathrm{km\,s^{-1}}$ and a standard deviation of ~ 3 $\mathrm{km\,s^{-1}}$. Shifts between spectral windows of different channels were larger (up to 130 $\mathrm{km\,s^{-1}}$).

The full widths at half maximum obtained were 9.9 ± 1.4, 10.9 ± 1.3 and 10.9 ± 1.2 pixels respectively for spectral windows from HIRS, MDRS, and LWRS (values are averages and standard deviations on all the corresponding windows). As expected, the spectral resolution is slightly higher for HIRS than for MDRS and LWRS. All the widths found were in the range 8 – 13 pixels. Note that for 14 spectral windows it was not possible to determine the LSF width because of the low signal-to-noise ratio; in these cases, the width was tuned to that obtained in the adjacent spectral windows.

4.2. Systematic effects

4.2.1. Overview

Error bars on column densities computed with the $\Delta\chi^2$ method (Sect. 3.6) include statistical *and* many possible systematic effects. The statistical aspect is obvious since the statistical error on each pixel is taken into account in the χ^2 computation.

Several approaches were used in order to reduce systematic errors. Some effects were treated as free parameters (Sect. 3.2). Some systematic effects are likely to be decreased by fitting simultaneously several different lines for a given element. It is possible that some of these effects affect our fits but the use of numerous different lines for a given element (see, for example, Table 3 for D I, O I, and N I) averages out any possible bias. In the same

spirit, effects which are totally or partially linked to instrumental effects are likely to be decreased by having data from multiple segments, multiple observations, and multiple slits fitted simultaneously. It is unlikely that one of these effects affect in the same manner a given line observed with what are essentially different instruments (different segments are used, through different slits, on different parts of the detectors). Finally, many possible systematic errors in the column density measurements are reduced by analyzing only unsaturated lines.

We list here the possible systematic effects which are treated using these four approaches:

- Free parameters:
  - continuum;
  - spectral shifts;
  - line spread function width.
- Simultaneous fit of several lines for a given element:
  - line blending;
  - oscillator strengths uncertainty;
  - continuum;
  - zero flux level determination;
  - fixed-pattern noise effects;
  - line spread function effects;
  - flux calibration;
  - wavelength calibration.

- Simultaneous fit of several segments:
  - continuum;
  - zero flux level determination;
  - fixed-pattern noise effects;
  - line spread function effects;
  - flux calibration;
  - wavelength calibration.
- Unsaturated lines:
  - number of interstellar components;
  - temperature of the clouds;
  - turbulence of the clouds;
  - shape and width of the line spread function.

4.2.2. Discussion of the effects and tests

In this section we discuss all the effects we investigated and we present some tests that we carried out in order to check the reliability of the error bars.

• *Line blending*

Line blending with unknown interstellar, stellar, or airglow features may affect the fit. However, such features are not present systematically for all lines of a given element. One exception is the He II stellar lines, falling systematically near the interstellar D I lines. However, no He II absorption is seen in the WD 2211−495 spectrum in the unblended lines at 1084.9Å or 992.3Å.

• *Oscillator strengths uncertainty*

Oscillator strengths (f) of D I lines are well known. However, this is not the case for some lines of other elements, such as O I or N I. If some f-values were found to be inaccurate, the fit of that line would stand out as a poor fit and the line would be rejected (*e.g.*, O I 1026.47Å). By fitting each line individually, we checked that each tabulated f-value is consistent with the others (none of them present an abnormal tabulated f-value). The range in column densities from fits to the individual lines retained in the sample presented a $\sim$ 20% dispersion around the value obtained with all the lines. Maybe some oscillator strengths are slightly inaccurate, but these errors should be small and average out in the final result.

• *Continuum placement*

The continua of the interstellar lines is given by the stellar continuum, possibly modified by instrumental effects (for example, one can see in Figure 1 the bump near 1165Å on LiF1, which is due to an instrumental artifact). For each spectral window, the continuum fitted by a polynomial is near the actual continuum but is probably not a perfect model. However, when the continuum is fitted independently for each line, in spectra obtained in each segment and each spectrograph aperture, it is unlikely that the average placement will be systematically higher or lower than the actual continuum.

We tested the possible systematic effect of the degree n of the polynomials by performing fits with values of n ranging from 1 to 14. Column densities obtained were consistent within the $2\,\sigma$ error bars. Thus, there is no strong dependence of the fit on the degree of the polynomials used to fit the continua.

Around the D I lines, the continuum is affected by the blue wing of the H I Lyman

line. In order to check the D I continuum levels found using polynomial approximations to the wings of the H I Lyman lines, we performed additional fits with Voigt profiles used to describe the H I lines. The value of N(D I) remained within the 2σ error bar, so we infer that continuum levels at the D I lines are not strongly dependent upon how the H I lines are modeled. We note that the H I column density is not constrained well by these fits since the H I Lyman lines lie on the flat part of the curve of growth.

Finally, we divided the spectra by the stellar model we computed (Sect. 3.4); fits of these normalized spectra produce column densities included within the $2\,\sigma$ error bars. Thus, no significant systematic effect linked to the continuum was found.

• *Zero flux level determination*

The zero flux level may be a function of wavelength. Simultaneous fits of different lines of a given element average out possible inaccuracies in the zero flux level determined from the bottom of the Lyman lines (Sect. 3.5).

We made extra fits in two extreme cases: doubling that correction (increasing the zero flux level by comparison with the best fit) and letting it remain zero. We also made fits where the zero flux level was a free parameter on each spectral window, with all windows fitted simultaneously. All these fits produced column density values again within the $2\,\sigma$ error bars.

• *Fixed-pattern noise effects*

Fixed-pattern noise is able to create false features that may artificially increase or decrease the intensity of an absorption line. The comparison of results for any single line, measured in different segments and apertures, allowed us to find lines affected by fixed-pattern noise. In the final fit, no lines were found to be in strong disagreement with the other ones so

these effects are small and average out in the fit.

• *Datasets*

In addition to fitting all the data simultaneously as described above, we also made fits to partial subsets of the total dataset presented in Table 2. These subsets were chosen to find possible time-dependent effects, segment to segment, channel to channel or detector to detector differences, and slit (HIRS, MDRS, LWRS) effects such as optical transmission, fixed-pattern noise, and airglow contamination (airglow intensity depends of the size of the aperture). All of the column densities found from these partial fits remained within the $2\,\sigma$ error ranges, so no significant effects were found. As expected, error bars obtained with only one of these subsets of data were larger than the ones obtained with the complete dataset.

• *Reduction procedure*

Fits were made from observations reduced with different spectra extraction, different wavelength calibration files, or different extraction windows on the two-dimensional images of the detectors. We found no significant effects due to the calibration uncertainties.

• *Selection of lines*

In order to identify possible effects on a given line (such as fixed-pattern noise right at the wavelength of a line or an erroneous f-value), we also fit each line independently of all others. No abnormal results were found for any line when compared to the composite fit results. In addition, this allowed us to identify saturated lines to be excluded from the final fit. For example, fits to the O I lines $\lambda\lambda 948.69, 971.74$ and 1039.23 (each line taken independently), with line strengths $f\lambda$ larger than $\sim$ 5Å, had large uncertainties and overestimated the value of N(O I) derived from weaker transitions. We rejected the

saturated lines using this objective criterion.

• *Selection of the species*

The D I, O I, N I, Fe II, and Si II lines were fitted assuming that all these species were in the same interstellar (neutral) cloud. The same radial velocity, turbulence, and temperature were assumed for all these species. This assumption may be incorrect if the species do not co-exist in the same regions along the sight line, which might be true if a significant amount of ionized gas is present. In order to test the possible systematic effect due to this assumption, we made extra fits including all these species but one. We also performed a fit including all the species but Fe II and Si II, which are the most likely ions to trace ionized gas. For all these fits, results for each column densities remained within the $1\,\sigma$ error bars.

• *Line spread function*

We used a simple Gaussian LSF in the fitting procedure and adopted a small zero flux level shift to account for weak, residual light contributed probably by a broad component of the LSF (Sect. 3.5). Note that the residual light does not affect the weak lines used in this study in an appreciable way. The robustness of this approach was tested on a simulated spectra made with a double Gaussian LSF; they were fitted with a simple Gaussian LSF and a tuned zero flux level, and the result was satisfactory (see below).

We also attempted to fit all spectral windows with a unique LSF width. Column densities obtained remained within the $2\,\sigma$ error bars for LSF full widths at half maximum included in the range 9 – 12.5 pixels; $\Delta\chi^2$ of the 9 and 12.5 pixel LSF solutions were large (> 200). Note that the minimum χ^2 was obtained for a 10.8 pixel width LSF. However, this χ^2 was greater by ~ 200 than that obtained with the LSFs left free to vary from one spectral window to the next, showing that as expected, the LSF does depend on the

wavelength, the segment, and the slit.

Finally, we performed fits with double Gaussian LSFs. We made tests using the LSF established by Wood et al. (2001), and other tests using free double Gaussian LSFs (Lemoine et al. 2001). Fits obtained with double Gaussian LSFs gave the same column densities within the $2\,\sigma$ error bars.

- *Temperature and turbulent velocity*

The values obtained for T and ξ are inaccurate (Sect. 4.1). We note, however, that the the impact of the uncertainty on the column densities is weak; for temperatures and turbulent velocities within 0 – 20000K and 1.5 – 7.0km s^{-1}, the column densities are consistent within the $2\,\sigma$ error bars. Hence, no effects on column densities due to T or ξ are significant, as expected from the fact that only unsaturated lines are fit.

- *Number of interstellar components on the sight line*

Fits were made assuming only one interstellar component on the line of sight, even if it is likely that several components are present along this $\sim$ 50 pc sight line. Since we use only unsaturated lines, assuming only one interstellar component should have no effect on the measurement of the total column densities. Fits obtained with up to five interstellar components along the line of sight gave the same total column densities within the $1\,\sigma$ error bars.

- *Simulation*

In order to test the various approaches of analyzing the interstellar lines from the *FUSE* spectra, an artificial spectrum was created for the *FUSE* Team members (Moos et

al. 2001). This simulated spectrum includes two interstellar clouds, He II lines in the stellar continuum, random noise, fixed-pattern noise, high frequency ringing, dithered wavelengths, background, and a double Gaussian LSF depending on the segment. This simulated spectra was fit in a blind manner using the method presented above (including only one interstellar component and simple Gaussian LSF). All the estimated column densities were in agreement with the inputs in the simulation within the $2\,\sigma$ error bars. This validates our approach and led us to a better understanding of the errors and the possible systematic uncertainties that might be present in our analysis.

• *Method*

Finally, a subset of the data presented here has been independently fitted using the procedure presented by Wood et al. (2001). Both approaches gave similar results, in agreement within $2\,\sigma$. The final values listed in Table 4 reflect the combined effort of these analyses.

5. Discussion

The O I and Ar I column densities presented here agree with the first *FUSE* results reported by Jenkins et al. (2000). Agreement is poor for N I, for which the value 14.02 ± 0.15 was reported by these authors. This early result was obtained with a lower number of lines and a lower signal-to-noise ratio. In the current study, the deficiency of N I along this sight line with respect to the value in B stars appears not to be as large as reported by Jenkins et al. (2000).

A value D/H $\simeq 1.5 \times 10^{-5}$ is obtained from the deuterium column density reported in Table 4 and the H I column density obtained from EUVE spectra: $\log N(\mathrm{H\ I}) = 18.76$

(Wolff et al. 1998). No error bar is available for this model-dependent H I estimate. We note that the far-UV spectrum of WD 2211−495 cannot be interpreted by using homogeneous H+He models (Marsh et al. 1997b), and that Holberg et al. (1998) quoted a different result, $\log N(\mathrm{H\ I}) = 18.3$, based on fitting the Lyman α line observed with by IUE.

Another way to estimate D/H is to use our present D/O measurement together with the accurate abundance of interstellar oxygen obtained by Meyer et al. (1998): $\mathrm{O/H} = 3.19(\pm0.14) \times 10^{-4}$. The low dispersion of O/H confirms that O I is a good tracer of H I in the Galactic disk. The Meyer et al. (1998) measurement was obtained from GHRS observations of 13 lines of sight ranging from 130 to 1500 pc, with most of them closer than 500 pc. This study examines interstellar clouds that are more distant than WD 2211−495. However, we note that the O/H value given by Meyer et al. (1998) agrees with that measured in the more local ISM (Moos et al. 2001). Using the Meyer et al. (1998) O/H value together with our new *FUSE* D/O measurement, we obtain $\mathrm{D/H} = 1.3(\pm0.4) \times 10^{-5}$ ($2\,\sigma$). Note that using the revisited value $\mathrm{O/H} = 3.43(\pm0.15) \times 10^{-4}$ from Meyer (2001), which adopt an updated O I oscillator strength, we obtain $\mathrm{D/H} = 1.4(\pm0.4) \times 10^{-5}$ ($2\,\sigma$).

In the same spirit, Meyer et al. (1997) determined from GHRS observations toward 7 stars the interstellar ratio $\mathrm{N/H} = 7.5(\pm0.4) \times 10^{-5}$. Adopting this value, our D/N value gives $\mathrm{D/H} = 3.3(\pm1.2) \times 10^{-5}$ ($2\,\sigma$). We can probably understand the difference between the O-based and N-based determinations of D/H in terms of the likelihood that N could be somewhat more ionized than H, whereas O and H are more strongly coupled to each other by charge exchange reactions. For example, Vidal-Madjar et al. (1998) have found toward G191−B2B that the O/H is perfectly consistent with the average of Meyer et al. (1998), while N/H is found to be a factor 2 smaller than the Meyer et al. (1997) ratio. In the case of WD 2211−495, this possibility is supported by the fact that Ar I is well below its expected column density in relation to both N I and O I, using the abundance ratios of these elements

in B-type stars as a reference (Cunha & Lambert 1992, 1994; Holmgren et al. 1990; Keenan et al. 1990). According to arguments presented by Sofia & Jenkins (1998), this condition indicates that a substantial fraction of the material is partially ionized by EUV photons that are allowed to penetrate the region. At the same time, if $n_e \gg n_{\rm H\,I}$ so that ordinary recombinations with free electrons dominate over charge exchange reactions of N II with H I, we might expect N I to behave in a manner similar to Ar I, *i.e.*, $n_{\rm N\,II}/n_{\rm N\,I} > n_{\rm H\,II}/n_{\rm H\,I}$, since the neutral forms of both N and Ar have photoionization cross sections larger than that of H. This inequality with the H ionization fraction is less likely to arise with O, since the charge exchange cross section of O II with H I (Field & Steigman 1971) is considerably larger than for N II with H I (Butler & Dalgarno 1979). An approximate indication of the expected magnitudes of the deficiencies of N I and Ar I is shown in Figure 2 of Jenkins et al. (2000).

In any case, an accurate H I column density value is needed to obtain a reliable $({\rm D/H})_{\rm ISM}$ measurement along this line of sight. Eventual observation of the Lyman α toward WD 2211−495 should provide this value since this line is not on the flat part of the curve of growth and therefore the damping wings can be used to measure N(H I) more accurately. As of now, D/O and D/N estimates appear to be more robust than D/H for the WD 2211−495 sight line.

Since H I, O I, and D I have nearly the same ionization potential, D/O ratio is an important proxy for the D/H ratio and its putative variations. D/O is very sensitive to astration, both from D I destruction and O I production (Timmes et al. 1997). If *FUSE* measurements of the D/O ratio toward other stars shows a relatively uniform value with low dispersion, it would argue in favor of D/H and O/H homogeneity in the interstellar medium. Indeed, the only other possibility would be that D/H and O/H vary precisely in the same way as to cause D/O to remain constant. It seems improbable since (i) O/H

appears to be uniform in the interstellar medium over paths of several hundred parsecs, and (ii) astration should lead to an anti-correlation of D I and O I abundances. An upcoming survey of D I and O I absorption along about 10 local lines of sight observed by *FUSE* should help determine whether the D/O ratio varies significantly from one sight line to the others (Hébrard et al. 2001). Initial indications are that the ratio does not vary substantially (Moos et al. 2001).

6. Conclusion

We have presented *FUSE* observations of the 905-1187 Å spectrum of the white dwarf WD 2211−495. The column densities of several ions were measured through simultaneous fits to the numerous unsaturated absorption lines detected in the four channels and through the three apertures. In particular, the ratios D/O = $4.0\,(\pm1.2) \times 10^{-2}$ and D/N = $4.4\,(\pm1.3) \times 10^{-1}$ ($2\,\sigma$ error bars) were measured. This result is discussed by Moos et al. (2001) together with other early *FUSE* deuterium results. Observations of the Lyman α absorption toward WD 2211−495 would help to constrain the D/H ratio along this sight line. Upcoming *FUSE* observations will help to determine if the D/H and D/O ratios vary locally. The answer to this question is critical to improving our understanding of the abundance of deuterium.

This work is based on data obtained for the Guaranteed Time Team by the NASA-CNES-CSA *FUSE* mission operated by the Johns Hopkins University. Financial support to U. S. participants has been provided by NASA contract NAS5-32985. French participants are supported by CNES.

REFERENCES

Allen, M. M., Jenkins, E. B., & Snow, T. P. 1992, ApJS, 83, 261

Barstow, M. A., Hubeny, I., & Holberg, J. B. 1998, MNRAS, 299, 520

Blitz, L. & Heiles, C. 1987, ApJ, 313, L95

Burles, S. & Tytler, D. 1998a, ApJ, 499, 699

Burles, S. & Tytler, D. 1998b, ApJ, 507, 732

Butler, S. E., & Dalgarno, A. 1979, ApJ, 234, 765

Chayer, P., et al. 2001, in preparation

Chengalur, J. N., Braun, R., & Burton, W. B. 1997, A&A, 318, L35

Cunha, K., & Lambert, D. L. 1992, ApJ, 399, 586

Cunha, K., & Lambert, D. L. 1994, ApJ, 426, 170

de Bernardis, P. et al. 2000, Nature, 404, 955

de Bernardis, P. et al. 2001, ApJ, submitted (`astro-ph/0105296`)

Epstein, R. I., Lattimer, J. M., & Schramm, D. N. 1976, Nature, 263, 198

Ferlet, R. et al. 2000, ApJ, 438, L69

Field, G. B., & Steigman, G. 1971, ApJ, 166, 59

Finley, D. S., Koester, D., & Basri, G. 1997, ApJ, 488, 375

Friedman, S. D. et al. 2001, ApJS, submitted

Galli, D., Palla, F., Ferrini, F., & Penco, U. 1995, ApJ, 443, 536

Hébrard, G., Mallouris, C., Ferlet, R., Koester, D., Lemoine, M., Vidal-Madjar, A., & York, D. 1999, A&A, 350, 643

Hébrard, G., Péquignot, D., Walsh, J. R., Vidal-Madjar, A., & Ferlet, R. 2000, A&A, 364, L31

Hébrard, G. et al. 2001, XVIIth IAP Colloquium, *Gaseous matter in galaxies and intergalactic space*, 19-23 June 2001, Paris, Edited by R. Ferlet et al., to be published; ApJ, in preparation

Hog, E., Kuzmin, A., Bastian, U., Fabricius, C., Kuimov, K., Lindegren, L., Makarov, V. V., & Roeser, S. 1998, A&A, 335, 65

Holberg, J. B. et al. 1993, ApJ, 416, 806

Holberg, J. B., Hubeny, I., Barstow, M. A., Lanz, T., Sion, E. M., & Tweedy, R. W. 1994, ApJ, 425, L105

Holberg, J. B., Barstow, M. A., & Sion, E. M. 1998, ApJS, 119, 207

Holmgren, D. E., Brown, P. J. F., Dufton, P. L., & Keenan, F. P. 1990, ApJ, 364, 657

Hubeny, I. & Lanz, T. 1995, ApJ, 439, 875

Jaffe, A. H., et al. 2001, Phys. Rev. Lett., 86, 3475

Jenkins, E. B., Tripp, T. M., Woźniak, P. ;. A., Sofia, U. J., & Sonneborn, G. 1999, ApJ, 520, 182

Jenkins, E. B. et al. 2000, ApJ, 538, L81

Keenan, F. P., Bates, B., Dufton, P. L., Holmgren, D. E., & Gilheany, S. 1990, ApJ, 348, 322

Kruk, J. W. et al. 2001, ApJS, submitted

Lallement, R., & Bertin, P. 1992, A&A, 266, 479

Laurent, C., Vidal-Madjar, A., & York, D. G. 1979, ApJ, 229, 923

Lehner, N. et al. 2001, ApJS, submitted

Lemoine, M., Vidal-Madjar, A., Bertin, P., Ferlet, R., Gry, C., & Lallement, R. 1996, A&A, 308, 601

Lemoine, M. et al. 1999, New Astronomy, 4, 231

Lemoine, M. et al. 2001, ApJS, submitted

Linsky, J. L. 1998, Space Science Reviews, 84, 285

Lubowich, D. A., Pasachoff, J. M., Balonek, T. J., Millar, T. J., Tremonti, C., Roberts, H., & Galloway, R. P. 2000, Nature, 405, 1025

Marsh, M. C. et al. 1997a, MNRAS, 286, 369

Marsh, M. C. et al. 1997b, MNRAS, 287, 705

Meyer, D. M., Cardelli, J. A., & Sofia, U. J. 1997, ApJ, 490, L103

Meyer, D. M., Jura, M., & Cardelli, J. A. 1998, ApJ, 493, 222

Meyer, D. M., XVIIth IAP Colloquium, *Gaseous matter in galaxies and intergalactic space*, 19-23 June 2001, Paris, Edited by R. Ferlet et al., to be published

Moos, H. W. et al. 2000, ApJ, 538, L1

Moos, H. W., Sembach, K. R. et al. 2001, ApJS, submitted

Morton, D. C. 1991, ApJS, 77, 119

Morton, D. C. 1999, private communication (http://www.hia.nrc.ca/staff/dcm/atomic_data.html)

Pounds, K. A. 1993, MNRAS, 260, 77

Prantzos, N. 1996, A&A, 310, 106

Pryke, C. et al. 2001, ApJ, submitted (astro-ph/0104490)

Rogerson, J., & York, D. 1973, ApJ, 186, L95

Sahnow, D. J. et al. 2000, ApJ, 538, L7

Sahu, M. S. et al. 1999, ApJ, 523, L159

Scully, S. T., Cassé, M., Olive. K. A., & Vangioni-Flam, E. 1997, ApJ, 476, 521

Sofia, U. J., & Jenkins, E. B. 1998, ApJ, 499, 951

Sonneborn, G., Tripp, T. M., Ferlet, R., Jenkins, E. B., Sofia, U. J., Vidal-Madjar, A., & Woźniak, P. ;. R. 2000, ApJ, 545, 277

Sonneborn, G. et al. 2001, ApJS, submitted

Stompor, R. et al. 2001, ApJ, submitted (astro-ph/0105062)

Timmes, F. X., Truran, J. W., Lauroesch, J. T., & York, D. G. 1997, ApJ, 476, 464

Tosi, M., Steigman, G., Matteucci, F., & Chiappini, C. 1998, ApJ, 498, 226

Vangioni-Flam, E., Olive, K. A., et al. 1994, ApJ, 427, 618

Vangioni-Flam, E., & Cassé, M. 1995, ApJ, 441, 471

Vennes, S., Thejll, P. A., Galvan, R. G., & Dupuis, J. 1997, ApJ, 480, 714

Vennes, S., Polomski, E. F., Lanz, T., Thorstensen, J. R., Chayer, P., & Gull, T. R. 2000, ApJ, 544, 423

Vidal-Madjar, A. et al. 1998, A&A, 338, 694

Webb, J. K., Carswell, R. F., Lanzetta, K. M., Ferlet, R., Lemoine, M., Vidal-Madjar, A., & Bowen, D. V. 1997, Nature, 388, 250

Werner, K., & Dreizler, S. 1994, A&A, 286, L31

Wolff, B., Koester, D., Dreizler, S., & Haas, S. 1998, A&A, 329, 1045

Wood, B. E. et al. 2001, ApJS, submitted

York, D. G. 1983, ApJ, 264, 172

This manuscript was prepared with the AAS LaTeX macros v5.0.

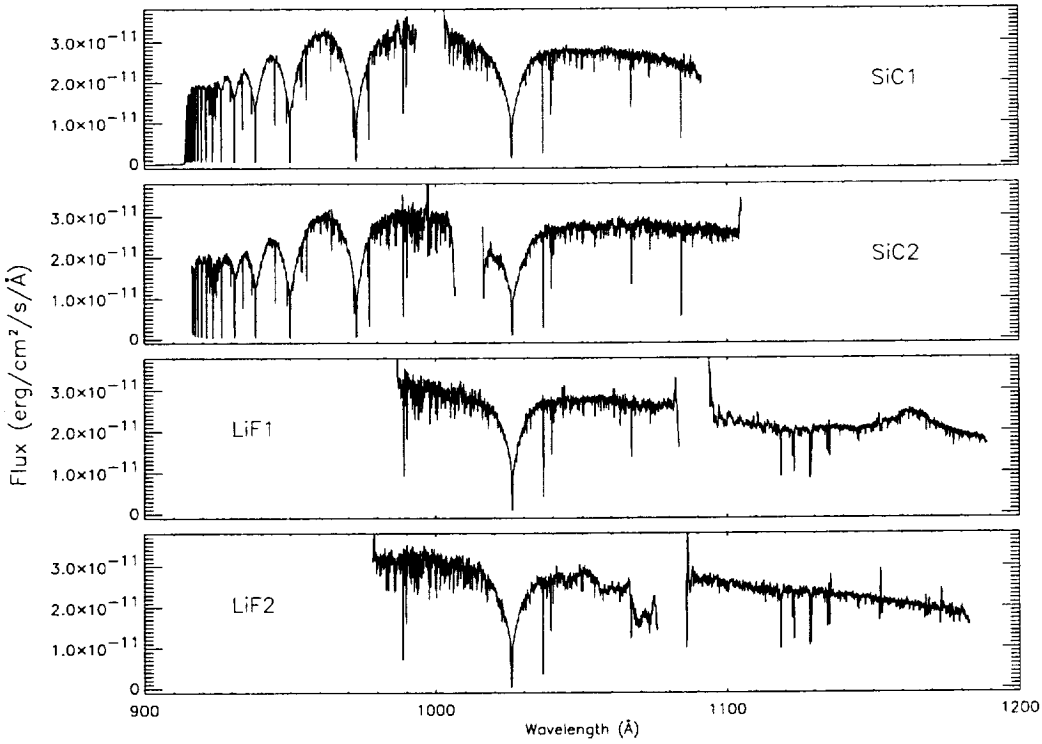

Fig. 1.— The eight segments of the *FUSE* WD 2211−495 spectra obtained through the large aperture (LWRS). Each channel (SiC1, SiC2, LiF1, and LiF2) is divided in two segments, separated by a gap. Similiar spectra were obtained for the two other slits (MDRS and HIRS); in total, $8 \times 3 = 24$ co-added spectra were used for the analysis. The bump in the LiF1 continuum at 1150Å is an instrumental artifact.

Table 1. Target Summary for WD 2211−495

Quantity	Value	Reference
Spectral Type	DA	1
l	345.79°	2
b	−52.62°	2
d (pc)	53	3
V	11.71	4
$U-B$	−1.21	4
$B-V$	−0.34	4
$T_{\rm eff}$ (K)	62,000	5
$\log g$ (cm s^{-2})	7.2	5
log(He/H)	< -4.0	1
$V_{\rm rad}$ (km s^{-1})	+33.9	6

References. — (1) Holberg et al. (1993); (2) Hog et al. (1998); (3) Vennes et al. (1997); (4) Marsh et al. (1997a); (5) Barstow et al. (1998); (6) Holberg et al. (1998).

Table 2. Log of the observations.

Obs. date	Obs. reference	T_{obs}[a]	N_{exp}[b]	Aperture[c]	CALFUSE[d]
1999.10.25	M1030303	4.2	8	LWRS	1.8.7
1999.10.31	M1030304	3.0	6	LWRS	1.8.7
2000.06.03	M1030305	5.2	11	LWRS	1.7.3
2000.06.29	M1030306	4.2	7	LWRS	1.7.7
2000.08.17	M1030307	5.3	11	LWRS	1.7.7
2000.10.24	M1030308	4.1	9	LWRS	1.7.7
2000.10.24	M1030309	5.1	10	LWRS	1.7.7
2000.10.24	M1030310	5.8	8	LWRS	1.7.7
2000.10.25	M1030311	6.1	13	LWRS	1.7.7
2000.10.25	M1030312	5.5	10	LWRS	1.7.7
2000.06.03	P1043801	16.5	35	MDRS	1.8.7
2000.06.02	M1030201	4.8	10	MDRS	1.8.7
2000.08.18	M1030202	4.8	10	MDRS	1.7.7
2000.10.24	M1030203	4.8	10	MDRS	1.7.7
2000.06.02	M1030101	4.3	9	HIRS	1.8.7
2000.08.18	M1030102	5.8	12	HIRS	1.8.7
2000.10.24	M1030103	4.3	9	HIRS	1.8.7
Total:[e]	17 obs.	93.8	188		

[a]Total exposure time of the observation (in 10^3 s).

[b]Number of individual exposures during the observation.

[c]LWRS, MDRS, and HIRS are respectively large, medium and narrow slits.

[d]Version of the pipeline used for spectral extraction.

[e]Totals for all datasets used in this study.

Table 3. D I, O I and N I lines included in the fit.

λ^a	f^b	#^{c}	λ^a	f^b	#^{c}	λ^a	f^b	#^{c}
D I			O I			N I		
1025.4434	7.91×10^{-2}	9	930.2566	5.37×10^{-4}	5	965.0413	4.02×10^{-3}	5
972.2723	2.90×10^{-2}	6	929.5168[d]	2.36×10^{-3}	5	964.6256	9.43×10^{-3}	6
949.4847	1.39×10^{-2}	3	925.4420	3.54×10^{-4}	3	963.9903	1.48×10^{-2}	3
937.5484	7.80×10^{-3}	1	924.9520[d]	1.59×10^{-3}	6	954.1042	6.76×10^{-3}	6
930.4951	4.82×10^{-3}	5	921.8570[d]	1.19×10^{-3}	3	953.9699	3.48×10^{-2}	6
925.9737	3.18×10^{-3}	3	919.9080	1.78×10^{-4}	3	953.6549	2.50×10^{-2}	6
916.9311	7.23×10^{-4}	2	919.6580[d]	9.47×10^{-4}	4	953.4152	1.32×10^{-2}	6
			916.8150[d]	4.74×10^{-4}	2	952.5227	6.00×10^{-4}	2
						952.4148	1.70×10^{-3}	2
						952.3034	1.87×10^{-3}	2
	total:	29		total:	31		total:	44

[a]Wavelength in vacuum at rest (in Å).

[b]Oscillator strength.

[c]Number of independent lines included in the fit (observed on different segments and through different slits).

[d]Triplet structure used (see Morton 1991; 1999)

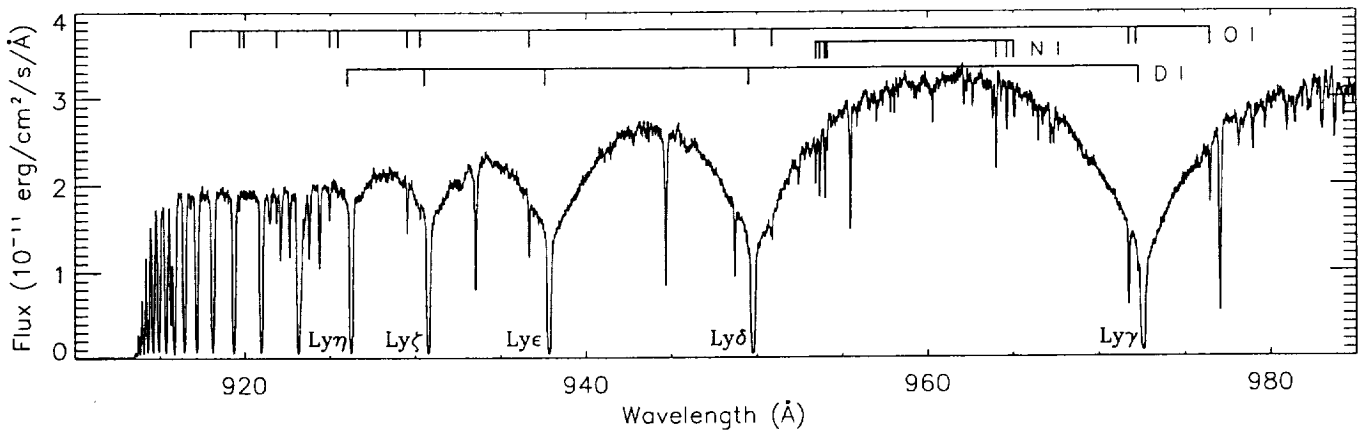

Fig. 2.— *FUSE* SiC1B spectrum of WD 2211−495 observed through the LWRS slit. Positions of D I, O I, and N I interstellar absorption lines are indicated.

Table 4. Total interstellar column densities.

species	$\log N(\mathrm{cm}^{-2})$[a]	species	$\log N(\mathrm{cm}^{-2})$[a]
D I	13.94 (±0.10)	Si II	14.00 (±0.15)
O I	15.34 (±0.08)	Ar I	12.82 (±0.10)
N I	14.30 (±0.06)	P II	12.05 (±0.20)
Fe II	13.25 (±0.15)	N II	14.6 (±0.3)

[a] 2σ error bars.

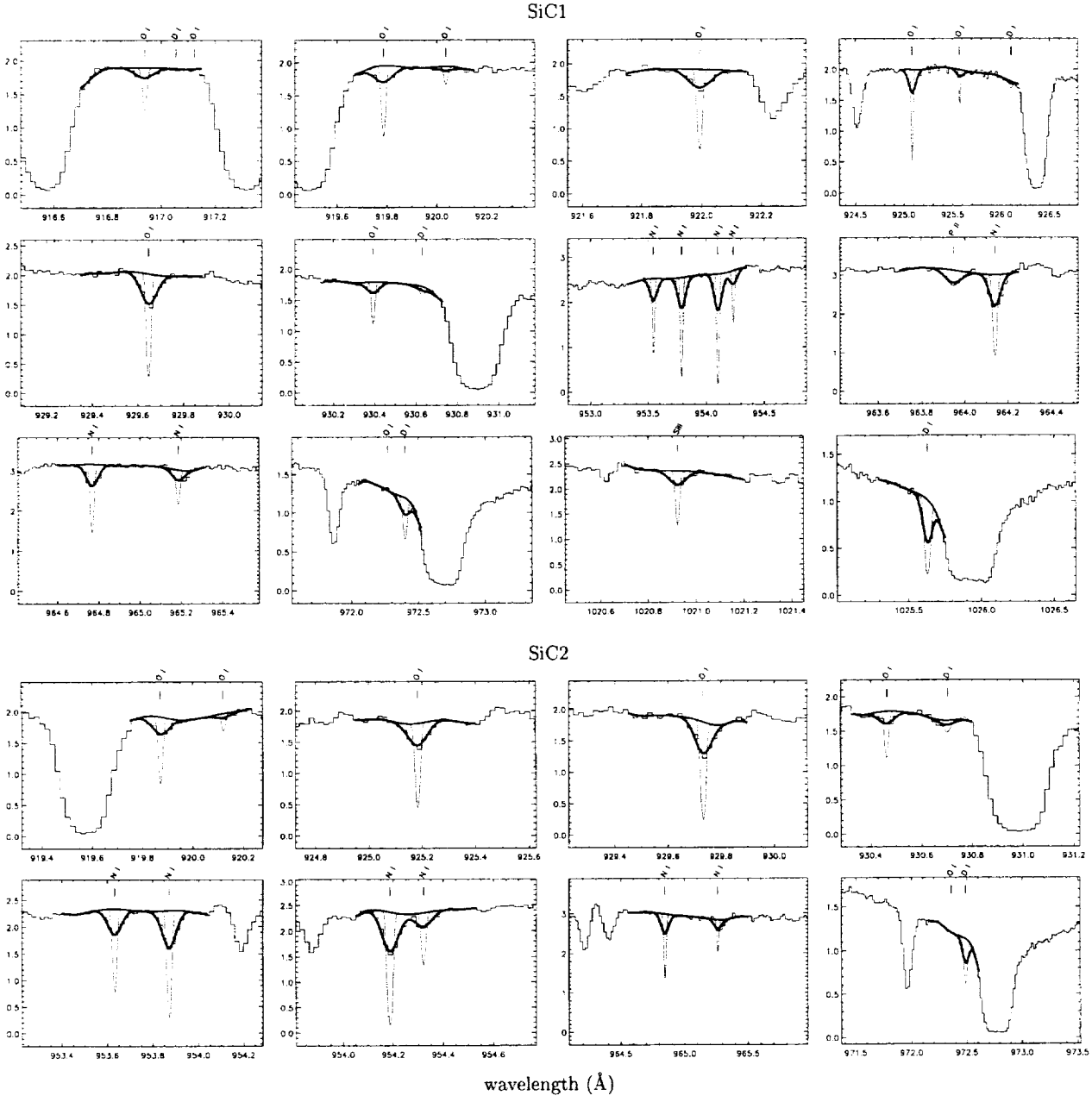

Fig. 3.— Plots of the fits to lines from the LWRS SiC data. The upper 12 spectra windows are from the SiC1 channel and the lower 8 spectral windows are from SiC2. Histogram lines are the data, the solid thick lines are the fits and continua, and the dotted lines are the model profiles prior to convolution with the LSF. Y-axis is flux in 10^{-11} erg/cm^2/s/Å.

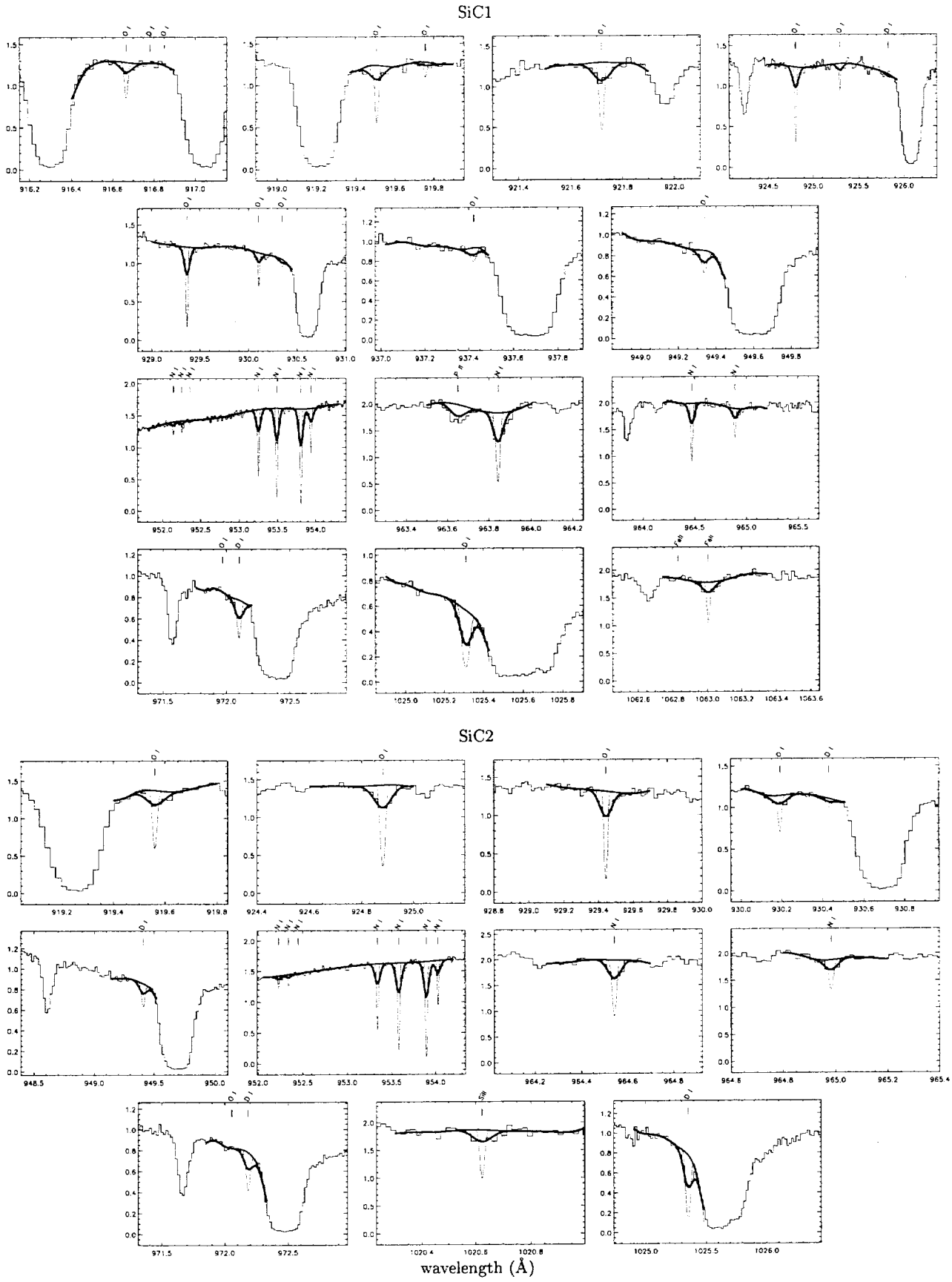

Fig. 4.— Same as Fig. 3, for MDRS SiC1 (upper) and SiC2 (lower) spectral windows.

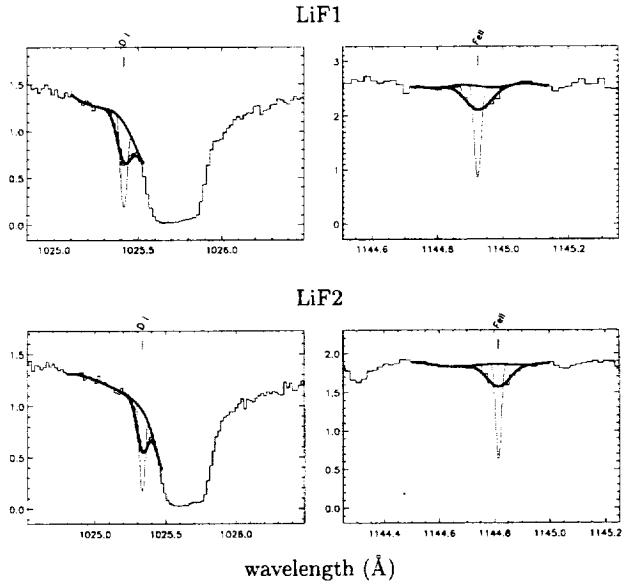

Fig. 5.— Same as Fig. 3, for MDRS LiF1 (upper) and LiF2 (lower) spectral windows.

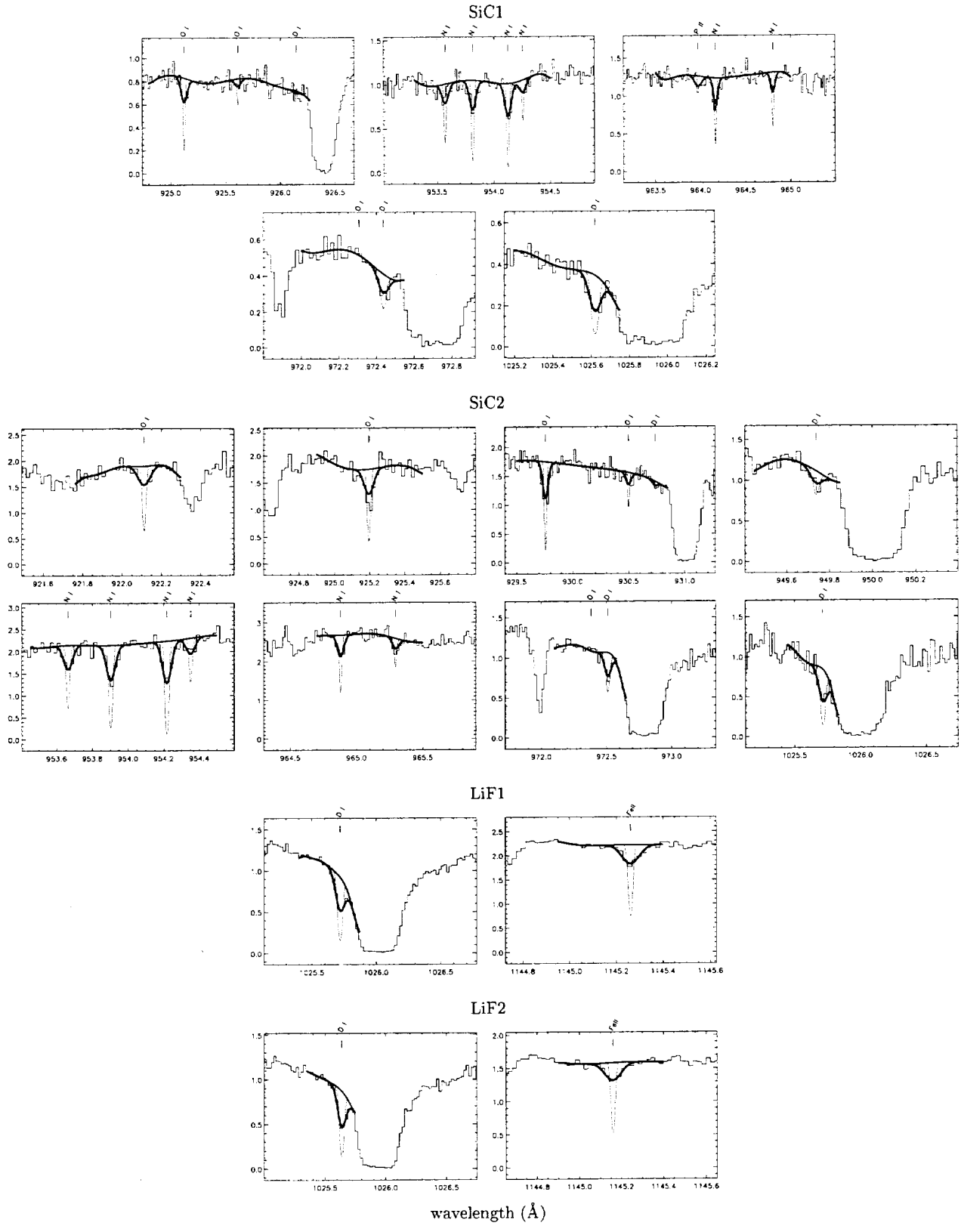

Fig. 6.— Same as Fig. 3, for HIRS SiC1, SiC2, LiF1 and LiF2 spectral windows.

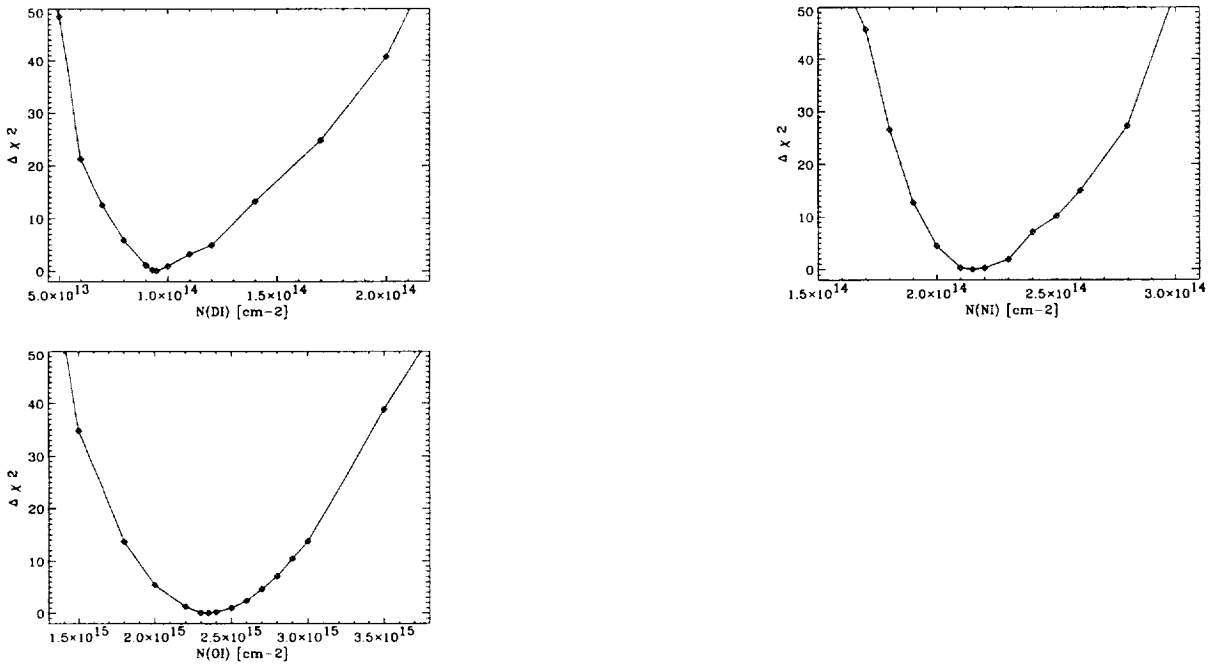

Fig. 7.— $\Delta\chi^2$ curves for D I, O I and N I. Each point on these curves corresponds to an individual fit, made with all the parameters free, but the D I, O I, or N I column density fixed. $\Delta\chi^2$= 25 corresponds to a $5\,\sigma$ error bar on the column density. $\Delta\chi^2$= 36 corresponds to $6\,\sigma$. $\Delta\chi^2$= 49 corresponds to $7\,\sigma$. χ^2 are rescaled on these plots (see Sect. 3.6).